JGR Atmospheres

RESEARCH ARTICLE
10.1029/2019JD031986

The 3rd AGILE Terrestrial Gamma-ray Flashes Catalog. Part II: Optimized Selection Criteria and Characteristics of the New Sample

C. Maiorana[1], M. Marisaldi[1,2], A. Lindanger[1], N. Østgaard[1], A. Ursi[3], D. Sarria[1], M. Galli[4], C. Labanti[2], M. Tavani[3], C. Pittori[5,6], and F. Verrecchia[5,6]

[1]Birkeland Centre for Space Science, Department of Physics and Technology, University of Bergen, Bergen, Norway, [2]INAF-OAS Bologna, Via Gobetti 101, I-40129 Bologna, Italy, [3]INAF-IAPS Roma, Rome, Italy, [4]ENEA, via Martiri di Monte Sole 4, I-40129 Bologna, Italy, [5]Space Science Data Center - Agenzia Spaziale Italiana, Via del Politecnico, s.n.c., I-00133, Roma, Italy, [6]INAF - Osservatorio Astronomico di Roma, Monte Porzio Catone, Roma, Italy

Abstract We present in this work the third catalog of terrestrial gamma-ray flashes (TGFs) by the AGILE mission and the new search algorithm that was developed to produce it. We firstly introduce the new selection criteria, designed from the characteristics of WWLLN-identified TGFs, and then applied on all data from March 2015 to September 2018. Association with sferics was performed by an independent search, described in a companion paper by Lindanger et al. (2020, https://doi.org/10.1029/2019JD031985). This search showed that many TGFs were not recognized by the existing selection algorithm, hence the need for this work. Several new selection criteria were tested and are compared in this paper. We then present the chosen selection criteria and the obtained sample, which includes 2,780 events and represents the most extensive TGF catalog available for the equatorial regions. Finally, we discuss the characteristics of this sample, including geographic distribution, intensity and duration, and seasonal variations.

This article is a companion to Lindanger et al. (2020), https://doi.org/10.1029/2019JD031985.

Key Points:
- A new set of selection criteria for AGILE TGFs is designed based on a lightning-associated TGF sample
- A sample of 2,780 events detected by AGILE over a 3-year period is presented, the largest sample to date across the equator
- Geographical, local time, and seasonal variability of the sample is discussed

Correspondence to:
C. Maiorana,
Carolina.Maiorana@uib.no

Citation:
Maiorana, C., Marisaldi, M., Lindanger, A., Østgaard, N., Ursi, A., Sarria, M., et al. (2020). The 3rd AGILE terrestrial gamma-ray flashes catalog. Part II: Optimized selection criteria and characteristics of the new sample. *Journal of Geophysical Research: Atmospheres*, *125*, e2019JD031986. https://doi.org/10.1029/2019JD031986

Received 6 NOV 2019
Accepted 31 MAR 2020
Accepted article online 8 APR 2020

1. Introduction

Terrestrial gamma-ray flashes (TGFs) are bursts of gamma photons produced inside thunderstorms and associated to lightning. They typically last for less than 1 ms, have energies up to a few tens of megaelectron volt, and are bright enough to be detected by particle detectors on spacecrafts. They were first recorded by the Burst and Transient Source Experiment (BATSE) instrument onboard the Compton Gamma Ray Observatory (CGRO) mission (Fishman et al., 1994), then by the Reuven Ramaty High Energy Solar Spectroscopic Imager (RHESSI) (Smith et al., 2005). They are now regularly observed by Fermi (Briggs et al., 2013), the Astro-rivelatore Gamma a Immagini Leggero (AGILE) (Marisaldi et al., 2010), and the Atmosphere-Space Interactions Monitor (ASIM) (Neubert et al., 2019), which MXGS instrument is specifically designed for the detection of TGFs. Many thousands of TGFs have been detected over the course of the years and catalogs have become an important tool available to the scientific community for general purposes: for population studies and to correlate TGF observations with other data, mainly ground-based lightning detection networks. Several TGF catalogs have been published so far: by RHESSI (Grefenstette et al., 2009), further improved in the work by Gjesteland et al. (2012); by Fermi (Roberts et al., 2018); and by AGILE (Marisaldi et al., 2014, 2015). Each of these missions are observing a slightly different population, due to the intrinsic differences in the detectors and orbits.

The AGILE mission is run by the Italian Space Agency (ASI) and is devoted to high-energy astrophysics (Tavani et al., 2009); it combines gamma- and hard X-ray imaging, for the simultaneous detection of photons in several energy bands. The primary goal of the mission is the study of the gamma-ray sky, but it was soon clear that also TGFs were detected by the Minicalorimeter (MCAL) instrument (Marisaldi et al., 2010). However, the dead time introduced by the anti-coincidence shield prevented the detection of events shorter than about 100μs, thus biasing the sample towards longer duration. Moreover, since the probability of association with the lightning sferic is inversely proportional to the duration of the TGF (Connaughton et al., 2013; Dwyer & Cummer, 2013) and is low for TGFs lasting more than about 150μs, no simultaneous association with lightning sferics were obtained. In March 2015, the anticoincidence shield was switched off for MCAL and the detection rate increased by almost one order of magnitude (Marisaldi et al., 2015).

The subsequent comparison with data from the World Wide Lightning Location Network (WWLLN) allowed the selection of a sample of TGFs simultaneously associated to lightning sferics, of which about half were not recognized by the offline selection, performed on ground. It was then clear that AGILE could benefit from a redesign of the TGF selection criteria and that this would lead to a substantial increase in the TGF detection rate. Here, we consider the AGILE 1st TGF catalog as the sample of 308 TGFs detected by MCAL between March 2009 and July 2012, prior to the inhibition of the anticoincidence shield, and published in Marisaldi et al. (2014) (available at https://www.ssdc.asi.it/mcaltgfcat/). We consider the AGILE 2nd catalog as the sample of 279 TGFs detected by MCAL between March and June 2015, following the inhibition of the anticoincidence shield, and published in Marisaldi et al. (2015) (available at https://www.ssdc.asi.it/mcaletgfcat/). The data set presented here include 2,780 events detected during the period between March 2015 and September 2018 and will be hereafter considered the 3rd AGILE TGF catalog.

We describe the data sets from AGILE in section 2. We then explain the method we have followed to design the new criteria in sections 3 and 4, a description of the old and new selection criteria and a description of the validation methods. In section 5, we present the obtained, new sample and we discuss the characteristics of said sample in terms of geographic and seasonal properties, compliance with theory and with other missions, limitations and improvements with respect to the older catalogs. An independent analysis of TGFs associated to lightning sferics detected by WWLLN is presented in the companion paper by Lindanger et al. (2020), hereafter referred to as L20.

2. Instruments and Data Sets

The AGILE payload includes several instruments, of which the MCAL is the main detector for TGFs. It is made of 30 scintillator bars arranged in two superimposed planes, with orthogonal orientation of the bars; see Labanti et al. (2009) for a detailed instrument description and (Tavani et al., 2009) for a complete description of the AGILE payload. Data collection takes place when a trigger is issued by the onboard trigger logic. The onboard trigger logic works on several timescales, from 293μs to 8 s. The most relevant timescale for TGF science is the shortest one, 293μs, for which a constant threshold of eight counts is set. Following each trigger, between about 6 and 10 s of data (depending on configuration setting) around the trigger time are then saved and downlinked. Since the trigger will include cosmic rays, statistical fluctuations and legitimate events (TGFs or cosmic Gamma-Ray Burst, GRB), those files are analyzed on ground to distinguish between the cases and identify TGF candidates.

One of the most relevant parameters to describe the sensitivity of an instrument is its effective area. This parameter depends both on photon energy and incoming direction; therefore, the total effective area depends on the spectrum of the source and the viewing angle. TGFs are known to exhibit spectral diversity (Mailyan et al., 2016). Moreover, the same source spectrum will result in different observed spectra at satellite altitude, depending on production altitude and distance between the source and the subsatellite point, because of photon propagation through the atmosphere. To assess the MCAL average total effective area for TGFs, we proceeded as follows. A TGF source spectrum consistent with a fully developed relativistic runaway electron avalanche (RREA) process is simulated. Photons are produced at 15-km altitude with angular distribution uniform on a cone with vertical axis and a half-cone angle of 40°. We chose a 15-km altitude because it is an adequate value for cloud top altitude in equatorial thunderstorms, as well as a value compatible with the analysis reported in Dwyer and Smith (2005) and Hazelton et al. (2009), although lower altitudes have been reported for the lightning leaders involved in TGF production (Cummer et al., 2015) and from radar observations associated to TGFs (Chronis et al., 2016). A 40° half opening angle at source is a value compatible with a large set of independent analysis (Carlson et al., 2007; Gjesteland et al., 2012; Hazelton et al., 2009). Photons are then propagated through the atmosphere, parameterized by the NRLMSISE model (Picone et al., 2002), up to satellite altitude by means of the GEANT4 toolkit (Agostinelli, 2003). Spectra for different distances between source and subsatellite point in the range between zero and 800 km have been simulated. These spectra were then used as input for the MCAL mass-model for different angles between the incoming photons direction and the normal to the detector plane. We call this angle θ. A large number of photons randomly extracted from the source spectrum was simulated. The total number of counts detected in MCAL was then divided by the number of incoming photons passing through the detector, and then multiplied by the detector geometrical area for the corresponding viewing angle. The obtained results are summarized in Figure 1, which shows the MCAL total effective area for a typical TGF as a function of the distance

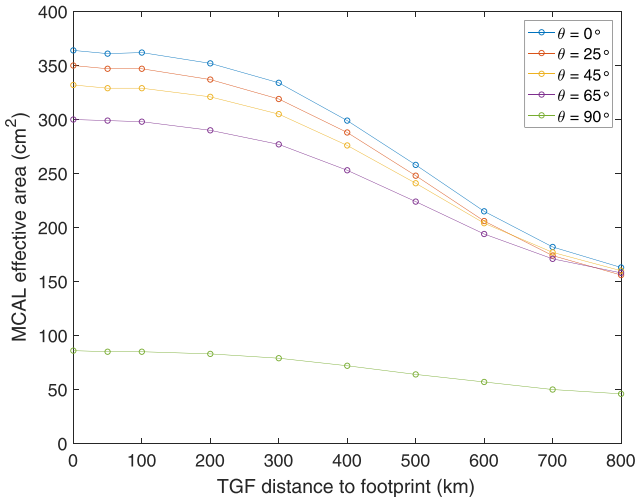

Figure 1. Total MCAL effective area for a typical TGF spectrum produced at 15-km altitude, as a function of the offset distance to the subsatellite point and the angle between the satellite pointing and the source location.

to the subsatellite point and the θ angle. This is equivalent to the convolution of a spectral model with a fluence of 1 ph/cm^2 with the appropriate detector response matrix, as done in the First Fermi TGF catalog (Roberts et al., 2018); see figure 4 therein. For practical purposes, Figure 1 allows to estimate the TGF fluence at satellite altitude, given the observed number of counts and the source distance to satellite footprint provided by an associated lightning sferics. A plot of the monoenergetic effective area can be found in Labanti et al. (2009) and Marisaldi et al. (2010). We only considered the θ angle because the MCAL response is only weakly dependent on the azimuth angle orthogonal to θ. We do not consider θ angles larger than 90° because then the photon flux interacts with the satellite structure, which is not accurately modeled, before entering the detector; therefore, the results are less reliable. We note also that in these computations, we did not consider the TGF flux, which may significantly deplete the effective area for very short and bright events, due to instrumental effects described in Marisaldi et al. (2019).

The general data set is divided into four data sets, summarized in Table 1, based on absolute timing accuracy and effectiveness of the anticoincidence shield (AC). More detailed information on those periods is in Lindanger et al. (2020). AC-ON refers to the first years of AGILE operations, with the onboard software configuration optimized for the detection of GRBs. We did not consider it for this work, as the presence of the anticoincidence shield poses some biases in the characteristics of the detected TGFs, which disrupt the homogeneity of the sample. Moreover, in this period, the TGF detection rate was about one tenth of that of the following periods and there are no WWLLN-associated events. The properties of the TGF sample collected in this period are described in (Marisaldi et al., 2014). A search for WWLLN associations in this period was carried out and discussed in L20. The reference (REF) period covers three months with optimal absolute timing accuracy after the inhibition of the AC for MCAL. The REF period presented here includes more data than the same period in Marisaldi et al. (2015), because we extended the REF period by two additional weeks for this study. The DRIFT period covers the span between July 2015 and December 2018. It is characterized by a failure in AGILE's internal clock, which caused a total loss of data for a few weeks at the beginning of the period, and a timing uncertainty on subsequent data of up to several tens of ms. A change in the onboard software configuration was implemented at the end of July 2016, motivated by the need for improved sensitivity to short electromagnetic counterparts associated with gravitational waves detected by LIGO-VIRGO (Ursi et al., 2019). Data from the first part of the period were taken with the same onboard configuration that was active during REF, and so they are safely comparable to data from the latter; in the following period AGILE can switch between two different configurations to accommodate telemetry necessities, at a single orbit level. The second configuration is more permissive, therefore allowing more triggers, which in turn increases the probability of recording a TGF. Finally, the 3D-FIX period starts in January 2018 and is characterized by a recovery of the internal clock precision. The software configuration flexibility is still ongoing as in the second half of the DRIFT period. Absolute timing accuracy at the microsecond level is a key requirement for the association of TGFs to lightning sferics, as discussed in details in L20.

Throughout the rest of this paper we call *WWLLN-identified* TGFs (WI) all those TGFs that are found by virtue of their association with a lightning sferic only; between the REF and 3D-FIX periods they form a

Table 1
Summary of the Data Sets

Name	Span	AC shield	Timing accuracy
AC-ON	28 February 2009 to 23 March 2015	On	~ 2μs
REF	23 March 2015 to 30 June 2015	Off	~ 2μs
DRIFT	01 July 2015 to 31 December 2017	Off	Several tens of ms
3D-Fix	17 January 2018 to 30 September 2018	Off	~ 2μs

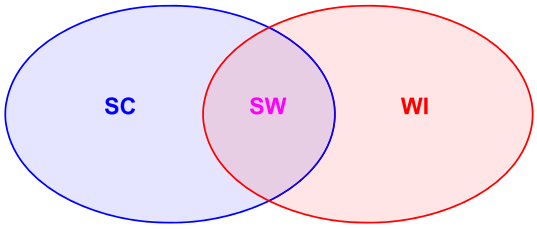

Figure 2. Venn diagram of the data sets used in this paper. SC: data set obtained with selection criteria. WI: WWLLN-identified data set. SW: SC subset with WWLLN identification.

sample of 278 events. We used the WI events as a starting point of our work: we analyzed their characteristics in order to model our selection criteria on them, with the purpose of refining those criteria and maximize the number of TGFs recognized, while at the same time rejecting as many false events as possible. Those events, and the method used to select them, are described in L20. L20 reports 282 WI events, as four additional TGFs were found after a refinement in their search algorithm; however, this happened when our analysis was already concluded; therefore, we decided against redoing it. We call *selection criteria identified* TGFs (SC) all those TGFs found based on the newly designed selection criteria, regardless of their association to lightning sferics. SC TGFs are the target of this paper, while WI TGFs are the target of the companion paper. A fraction of the SC data set is associated to sferics and therefore included also in the WI data set. We refer to this intersection between the two data sets as *selection criteria and WWLLN identified* TGFs (SW). Figure 2 shows a schematic representation of the TGF data sets used in this paper.

3. Observables and Original Selection Criteria

As mentioned in section 2, triggered data still need to be processed in order to distinguish TGFs from other types of events. We start our search by scanning all the available data streams in search for clusters of counts, irrespective of the onboard trigger. We call a "cluster" a streak of at least 6 counts in the detector occurring within 300μs. We then consider related counts all those that come no later than 300μs from the previous one. This may cause the cluster to continue outside of the original trigger window, which is not a problem since we have at least six seconds of data around each trigger. All count groups that originate from an onboard trigger in the 293μs time window must be selected as clusters by the onground analysis (threshold is either 8 or 7 counts for the onboard logic); however, the ground search can identify many more clusters in the data stream that did not give rise to an onboard trigger. It is possible to calculate several parameters for each cluster, which are then used to determine whether the cluster is classified as a TGF or not. The parameters that we chose to evaluate are the following:

1. Maximum energy ($E_{\max}$)
2. Mean energy (E_{avg})
3. Median energy (E_{med})
4. Hardness ratio (HR)
5. Number of counts (N)
6. Uniformity (number of detector segments hit)
7. Duration (Δt)
8. Count rate ($F = N/\Delta t$)

Given the intrinsic spectral hardness of TGFs, energy-related observables are key parameters to disentangle TGF candidates from other, softer events. Maximum energy ($E_{\max}$) is the largest energy measured among the single counts in the cluster. Mean and median energy are cluster-wide quantities; median energy is favored over mean because it is less sensitive to statistic fluctuations. HR is the ratio between counts of energy above 1.4 MeV and the ones below. The threshold value of 1.4 MeV was chosen for historical, hardware-related reasons and could in principle be adjusted.

We define the duration of the cluster (Δt) as the time difference between the first and last event. This is a very coarse measure of duration and will be refined for those clusters subsequently labeled as TGFs. Uniformity, or detector occupation, is a measure of the spreading of the events belonging to a single cluster across the detector planes: Since TGFs at satellite altitude can be approximated to a plane wave, we expect them to involve the whole detector, thus having counts in all of its sectors. Uniformity is related to the spatial symmetry of the cluster counts over the detection planes and is a very efficient way to discard electronic noise and cosmic rays, which both tend to show counts clustered in localized parts of the detector. Uniformity can be measured in several ways. Here, we divide the two MCAL planes in four parts each, for a total of eight segments, and count how many segments are hit by at least one count.

Table 2
The Number of WI TGFs Failing on Any of the Selection Criteria

Criterion	TGFs failing
Any	146
Max E	70
HR	21
n counts	64
Uniformity	14

The original selection criteria (CO, Marisaldi et al., 2014, 2015) were defined by setting thresholds and cuts on four of these parameters, as follows:

1. $E_{\max} \leq 30\,\text{MeV}$
2. $HR \geq 0.5$
3. $N \geq 10$
4. Uniformity criterion: at least one count in each of the four quadrants of MCAL, where a quadrant is defined as half a detection plane, that is, two adjacent segments

4. Methods

In order to improve the original criteria, we developed and tested several, new sets of selection criteria (each labeled CN_x in the following) considering more observables and adjusting the threshold according to the characteristics of the WI data set, following the subsequent steps:

1. Identify which of the original criteria failed most often on the WI data set.
2. Definition of a set of new selection criteria based on the previous diagnostics and application to the full data sets.
3. Validation of the TGF candidates obtained with each selection set.
4. Refinement of the new selection criteria based on validation results.

These steps are detailed in the following paragraphs.

4.1. Original Criteria Diagnostic on WI Data Set

TGFs are considered to have a WWLLN association when there is a sferic no more than 0.5 ms apart; we found 111 events in the REF period and 167 in the 3D-FIX, for a total of 278 (L20). The characteristics of those events are independent from any selection criteria, except for the fact that short TGFs are more likely to have an association (Connaughton et al., 2013) (more on this in paragraph 5.3). We then applied the CO to WI events to see where they failed. The results are shown in Table 2. Criteria on HR and uniformity are the ones working best. We manually examined the events rejected by these criteria and they all were very weak events that would not be recognized as TGFs if not for the WWLLN association. The most problematic criterion appeared to be the cut in maximum energy. The limit value of 30 MeV was set to reject not only cosmic rays but also high-energy candidates of uncertain origin, as described in Marisaldi et al. (2014); however, results shown in Table 2 indicate that many real TGFs exhibit counts with reconstructed energy above 30 MeV, although this energy estimate is most likely due to pileup effects. (Marisaldi et al., 2019) reports a model of the electronic front-end responsible of pileup and deadtime. The problem is complex, as it originates from the behavior of both analog and digital electronics, and cannot be determined by one parameter only. Therefore, we decided to set a higher upper limit to maximum energy and explore other possible ways of rejecting cosmic rays. The criterion on number of counts is also too strict, but allowing for a too low number of counts means increasing the number of false events greatly.

4.2. Definition of a Set of New Selection Criteria

Starting from the CO and according to the value ranges of the WI, we designed several new variations of the selection criteria, shown in Table 3. All these criteria were applied to the full data set, each resulting in a set of candidate TGFs, which need to be assessed for reliability.

Table 3
The Different Sets of Selection Criteria

Name	Uniformity	HR	E_{med}	E_{max}	n counts
CO	Yes	≥ 0.5	–	≤ 30	≥ 10
CN_1	Yes	≥ 0.5	–	≤ 120	≥ 10
CN_2	Yes	≥ 0.5	–	≤ 30	≥ 9
CN_3	Yes	≥ 0.5	–	≤ 120	≥ 9
CN_4	Yes	–	≥ 0.5	≤ 30	≥ 10
CN_5	Yes	–	≥ 0.5	≤ 120	≥ 10
CN_6	Yes	–	≥ 0.5	≤ 30	≥ 9
CN_7	Yes	–	≥ 0.5	≤ 120	≥ 9

4.3. Validation

After applying a set of selection criteria to the whole data set, we need a way of evaluating the true-versus-false events ratio and, more generally, the goodness (reliability) of the obtained TGF candidate set. We applied three methods, of which two qualitative and one quantitative:

1. Longitude distribution of the sample
2. Local time distribution of the sample
3. Quality factor

The two qualitative and most straightforward ways take advantage of the fact that we know where and when to expect TGFs. Being produced by thunderstorms, they are more frequent above equatorial mainland and during early morning or late afternoon. We then expect our candidates to be clustered at longitude values corresponding to land and to follow a modulation with local time. Background cosmic particles events, i.e. events uncorrelated to thunderstorm activity, on the other hand, would appear as a constant baseline, at best slightly modulated by magnetic latitude in the case of the geographic distribution. As a quantitative measure, we compared the average detection rate with the one in a region with scarcity of storms. This method was first used by Briggs et al. (2013) and then in Marisaldi et al. (2015). The control regions extends from -110 to -140 degrees of longitude. The high-density region is the sum of the three "lightning chimneys": the African one from −10° to 30°, the South-East Asian one from 100° to 150°, and the Central American one from −90° to −60°. Hereafter, we call Quality Factor (QF) the ratio between the number of events in the control region and the high-density region. The QF is not normalized for the different span of those two regions, as there is no objective way to estimate how many of the control region events are actually noise: being AGILE on an equatorial orbit, we still expect a small number of thunderstorms even above the open ocean. As another quality flag we consider also the fraction of the WI data set identified by the new selection criteria. The results of the validation will be presented in section 5.

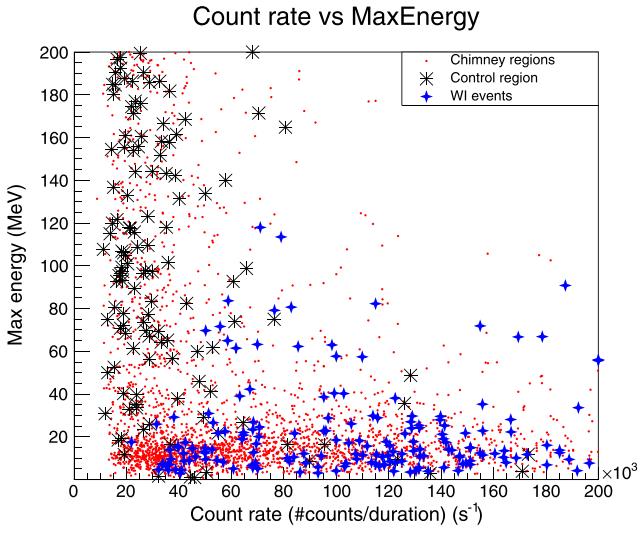

Figure 3. The count rate versus max energy for events occurring in the chimney regions and in the control region.

4.4. Criteria Refinement

None of the CN gave satisfactory results in the control region; we then proceeded to analyze those events more closely to understand their origin.

We considered the ratio between the number of counts and the duration, which represents a rough estimate of the count rate of the event. In Figure 3, we show this for events from the control region and events from the three chimneys, and we assume for this purpose that all events in the control region are false events, while all the others are TGFs. The figure shows that false events tend to cluster at low count rate and high energy. TGFs, on the other hand, are mostly low count rate and lower energy. We can verify this by plotting the geographic distribution of events according to count rate and energy: low-count rate, lower-energy events follow the expected longitude distribution for TGFs, peaking above equatorial mainland, while low-count rate, high-energy events are uniformly distributed. High-count rate events also follow the three-chimney structure,

Table 4
Efficiency of Each Set of Selection Criteria

Name	Number WI selected	Total events selected	Quality factor
CO	121	2,354	18/1966
CN_1	166	2,686	0.011 (26/2,221)
CN_2	158	2,930	0.023 (52/2,276)
CN_3	199	3,531	0.029 (78/2,659)
CN_4	146	2,505	0.009 (20/2,082)
CN_5	177	2,834	0.012 (28/2,335)
CN_6	172	2,962	0.016 (37/2,369)
CN_7	213	3,439	0.019 (52/2,703)

although the pattern is slightly less clean, possibly because of the lower statistics. Remarkably, WI TGFs tend to have higher values of count rate: This is explained by the shorter duration of WI events, as explained in Connaughton et al. (2013) and L20. Energies greater than 30 MeV can be either due to real photons, pileup (Marisaldi et al., 2019) or the presence of counts from cosmic rays, and confirm the need of relaxing the criteria on maximum energy. This led to the introduction of an additional, empirical criterion, as a way to remove even more false events: for count rate below 50 kHz, we only allow events with maximum energy up to 30 MeV. For higher values of count rate, we allow energies up to 120 MeV. We justify this by considering that the probability of pile-up increases for higher values of count rate. All of those thresholds were found empirically, from the values of the studied events, in order to optimize the ratio of events in the active and control regions. The 30-MeV cut on energy also happens to be consistent with the energy cut in the CO. We then reapplied the set of refined criteria to the full data set. This added criterion affects only the CN where the cut on maximum energy was previously set to 120 MeV.

5. Results and Discussion

5.1. Choice of Selection Criteria

Table 4 shows an overview of all the different selections we tested concerning number of WI events selected, total number of TGF events, and the quality factor discussed in section 4.3. Here, we count each cluster as a single event, regardless of its possible association with a multipulse event, as we are considering the efficiency of the criteria in selecting clusters. The multipulse events are discussed in section 5.5. None of the chosen set of criteria optimizes all three parameters reported in Table 4; therefore, a trade-off is necessary. We decided to give more weight to the cleanliness of the sample (a low quality factor), first, and the total number of WI events selected as a second requirement. In this regard, the selection set that proved to offer the best balance is CN_5:

1. Number of counts ≥ 10
2. $E_{\mathrm{med}} \geq 0.5$ MeV
3. At least one count in each quadrant
4. If count rate < 50 kHz, $E_{\mathrm{max}} \leq 30$ MeV
5. If count rate ≥ 50 kHz, $E_{\mathrm{max}} \leq 120$ MeV

This is the set of selection criteria adopted for the 3rd AGILE TGF catalog. All results shown in the rest of this paper correspond to the TGF sample obtained with these criteria. The actual number of events selected is 2,780, as some of the 2,834 turned out to be part of a multipeak event. The sample obtained from this selection represents the largest TGF data set over equator currently available.

5.2. Improvement of the New Sample

As stated in section 1, one goal of this study was to include in the sample those events that were recognized as TGFs by their association with WWLLN, but not from the offline selection algorithm. The old catalog included 279 TGFs in the REF period; in contrast, the new one has 457 TGFs in the REF period and 2,780 in total. Of these 2,780, 177 are associated with a WWLLN sferic. The new criteria have improved the inclusion of high-energy events in particular, thus allowing for a maximum energy of up to 120 MeV. Those high energy counts are however a product of pileup, which affects short and high-fluence events. The analysis reported in Marisaldi et al. (2019) shows that these events are still compatible with a standard RREA

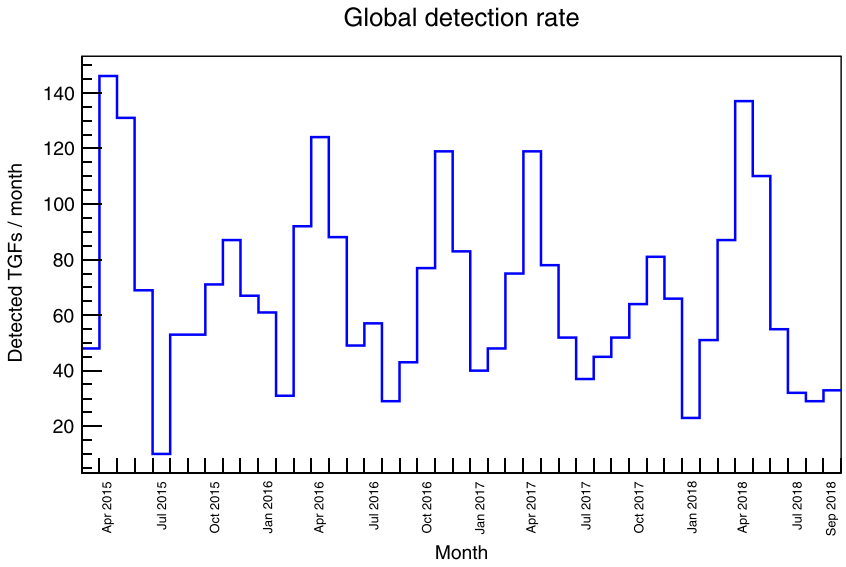

Figure 4. The detection rate of AGILE over the course of the 3 years covered by the catalog. The dip around July 2015 is due to the clock failure, the one at January 2018 corresponds to another period of noisy data.

spectrum, with maximum energy of few tens of MeV, provided that the instrumental effects are carefully accounted for. However, the events affected by pileup are real TGFs and reliable in all other aspects; they should just be considered carefully when calculating the energy spectra. We also found one Terrestrial Electron Beam event, which is described in details in L20. We decided to keep the threshold on the total number of counts relatively high. Lowering the threshold on number of counts, while greatly increasing the number of selected TGFs (see Table 4), was also introducing a large number of false events, as evidenced by the worsening of the quality factor. Those noise events appeared unrelated to the thunderstorm peaks in the longitude plot and had different distributions of their parameters, namely, the energy (i.e., homogeneous instead of Gaussian-like). The additional criterion on count rate alone was not sufficient to completely eliminate them in CN_3 and CN_7, but we would have needed more complex, probability-based algorithms; we preferred discarding those sets. Figure 4 shows the global detection rate for the period covered by the catalog: March 2015 to September 2018. The average detection rate does not change over the years, showing that the behavior of the selection criteria remains consistent along the seasons. The empty period around July 2015 corresponds to the clock failure between the REF and the DRIFT periods. The periodic variation is mostly due to the seasonal variability. The seasonal behavior of the TGF rate is further discussed in section 5.6

5.3. Limitations of the New Sample

While our aim was to be as inclusive as possible with the TGF selection, the new sample is likely affected by limitations and bias. The most obvious one is that we based our criteria on the characteristics of relatively few WWLLN-identified TGFs, detected over a period of twelve months (three in the REF period and nine in the 3D-FIX). It has already been proved that the probability of association with sferics decreases as the duration of the TGF increases, which means that our sample may be biased towards shorter TGFs. We avoided using the duration as a selection criteria for this reason, and also for the difficulty in defining it in an objective way, but shorter TGFs may be different from longer ones also in other ways. Moreover, all reference TGFs were detected during the spring and summer months (REF and 3D-FIX periods; see Table 1) and may, in principle, have specific characteristics different from the ones of TGFs produced by thunderstorm systems developing in other seasons, that is, in different atmospheric conditions. Seasonal behavior is discussed in more detail in section 5.6. Finally, as mentioned in section 5.2, we refrained from including the faintest TGFs, to avoid introducing more false events in our sample; however, this led to the loss of some valid TGFs. It is still possible to recover those events, but it will require a much more sophisticated approach, which was outside the scope of this work. Very faint TGFs, due to the very low number of counts, do not allow robust estimate of the global parameters and a reliable spectral analysis.

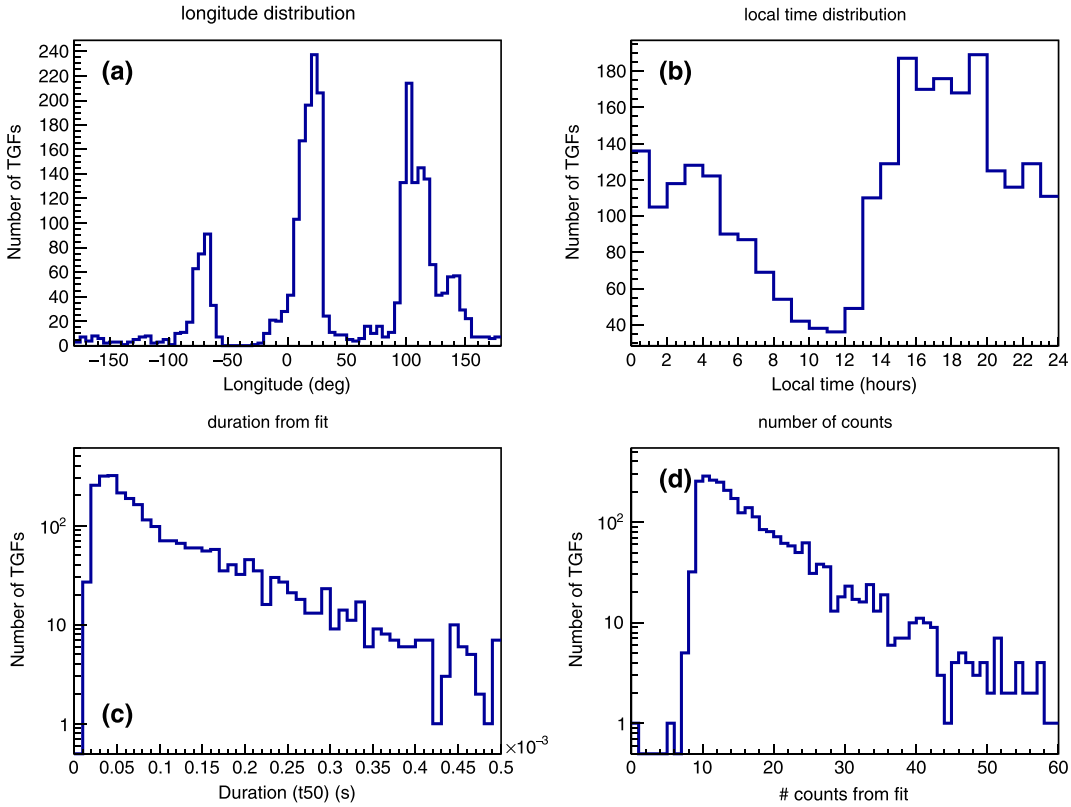

Figure 5. (a) Longitude and (b) local time distribution of the whole data set obtained with the CN_5 criteria set. (c) Duration (t_{50}) distribution of the sample. (d) Intensity (from maximum likelihood fit) distribution of the sample.

5.4. Impact of the Onboard Trigger Logic Configuration

As already stated, the TGF search was applied to the full data stream collected which includes, for every onboard trigger, a span of about 6 to 10 s of data (depending on the configuration of the onboard trigger logic) around the trigger time. Therefore, although the search was not based on the triggers, it was unavoidably affected by the trigger logic configuration, just because the data availability relies on the issuing of an onboard trigger. This, together with the fact that the onboard trigger configuration has changed significantly during the time period considered in this work, made us consider whether the trigger logic configuration is somehow biasing our sample and the associated results. We therefore carried out a retrospective analysis to understand, given the selected TGF sample, which of the trigger time windows was responsible for the data span in which the TGF was found, and the time separation between the TGF and the trigger. The results show that in 96% of the cases the trigger has fired on the 293μs time scale, the sub-millisecond trigger; moreover, in 94% of the cases, the time separation between the TGF time and the trigger time is < 16 ms, indicating that the TGF itself was the cause of the trigger. This is an important result because the sub-millisecond trigger logic configuration has been kept constant during the full time span considered in this work. The static threshold was lowered from 8 to 7 counts from September 2016, but this is not significantly affecting the results since only events with at least ten counts are considered by the chosen selection criteria. These considerations indicate that the AGILE sensitivity for TGFs is uniform along the orbit and during the full time span considered in this work. This is a relevant information to consider when attempting quantitative comparisons with other data sets or when addressing the seasonal variability of the sample.

The 16-ms time window, the one most heavily affected by the introduced configuration changes, is responsible alone for only 2% of the TGFs. Of these, 95% is detected far from the trigger time, meaning that the TGF did not cause the trigger on such a long time scale, but was indeed detected by chance within the available data span.

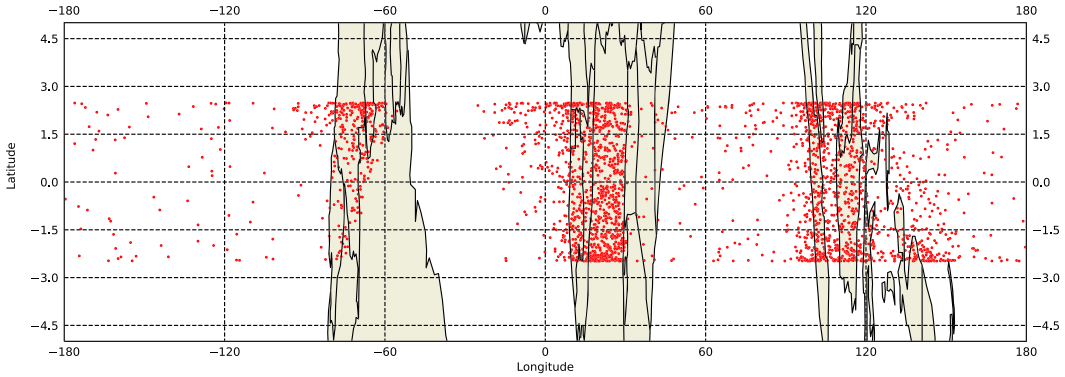

Figure 6. A global map of the catalog sample. The empty area over South America corresponds to the SAA.

5.5. Global Characteristics of the Sample

Figure 5 shows the global distributions of longitude (a), local time (b), duration (t_{50}) (c), and number of counts (d) for the full data set. The duration and intensity shown in panels (c) and (d) are the ones obtained from the maximum likelihood procedure described in L20, not the ones used in the criteria development phase and listed in section 3. The quantities from fit are consistent with the previous catalogs (Marisaldi et al., 2015), but were only calculated on the final sample, to avoid influencing the selection criteria. The initial, operational definition of duration was only used during the development of the criteria and is not included in the publicly available database. We note that in some cases the number of counts shown in panel (d) is lower than 10, which is apparently in contrast with the threshold for TGF identification. This is because the plotted parameter is the TGF intensity resulting from the integral of the maximum likelihood Gaussian fit; therefore, it accounts for both the model and background subtraction. The catalog also includes 95 multipulse events (3.4% of the sample), but only the first peak of each event was considered for this plot. Each multipulse event was analyzed manually, as some peaks were not recognized as independent clusters by the automatic selection and had to be retrieved from the raw data. As a consequence, many of such trailing peaks have properties that do not satisfy the selection criteria (specifically, many of them had fewer than 10 counts) and were therefore excluded from the plots, to avoid confusion. The catalog includes all pulses as single entries, appropriately flagged to distinguish between first and trailing pulses, bringing the total number of entries to 2,903. The fraction of multipulse events is in accordance with Mezentsev et al. (2016), for RHESSI, and also with the previous results for AGILE (Marisaldi et al., 2014), although less strictly. It is not, however, compatible with Foley et al. (2014), which reports for Fermi a much higher occurrence rate; an explanation for this discrepancy is yet to be found. The multipulse TGFs have different shapes and a number of peaks which ranges from two to five. The catalog also includes 128 potential multipulse, that is, events with an irregular light curve that was nonetheless not univocally classifiable as multiple. Those events are also labeled in the catalog, but were treated as normal events.

Finally, Figure 5a also shows a fourth lightning enhancement between -180 and -150 degrees of longitude. This feature is visible in the LIS/OTD lightning maps (Albrecht et al., 2016) and was already reported by Fabró et al. (2015) but the characteristics of TGFs occurring in this area are yet to be studied.

5.6. Geographic and Seasonal Variability

The high number of events detected in a small latitude span result in a high density of events, which in turn allows a fine binning for a study of seasonal and geographical variability. In order to perform this study, we selected the events occurring in the high-density regions (Central Africa, Oceania and Central America, as defined in section 4.3). All the following plots include the complete data set, without distinction of the periods and excluding the trailing peaks of multipulse events.

Figure 6 is a world map with all the events in the catalog. TGFs clearly prefer coastal and inland areas, but there are also several events over the ocean: lightnings over ocean are in fact more frequent at equatorial latitudes than they are elsewhere. The completely empty area over South America corresponds to the South Atlantic Anomaly (SAA), where the MCAL trigger logic is not active. This also explains the smaller number of events observed over South America, as it is noticeable in all following plots. Figure 7 (right panels) shows the local time distribution of the events in the three regions. Africa shows a higher rate of events occurring

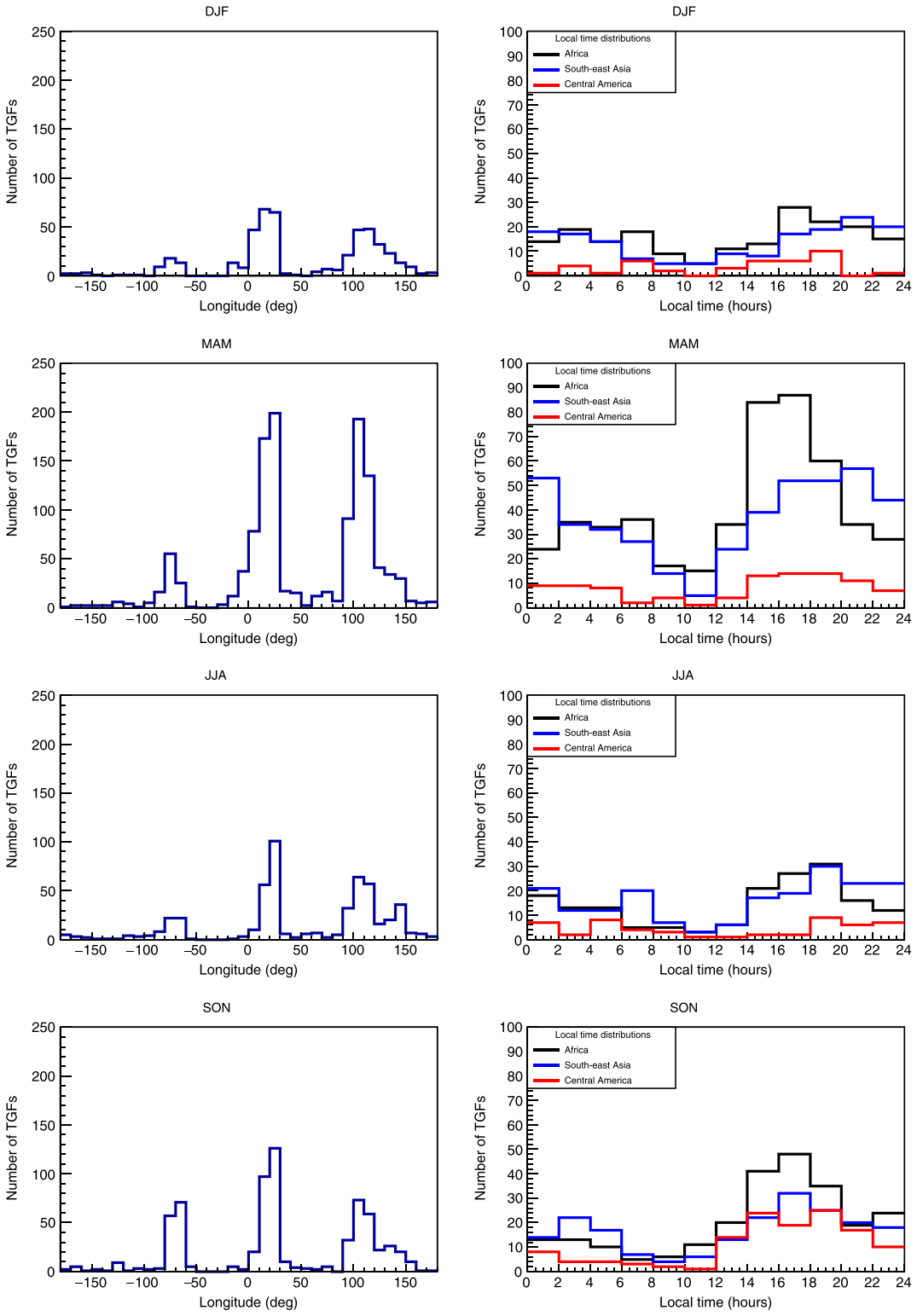

Figure 7. The geographic and local time distributions of all events in the catalog divided by season; the local time plot also divides the events by geographical region. The differences in both distributions follow local and seasonal weather patterns. Seasons are defined as three winter months (DJF), three spring months (MAM), there summer months (JJA) and three fall months (SON).

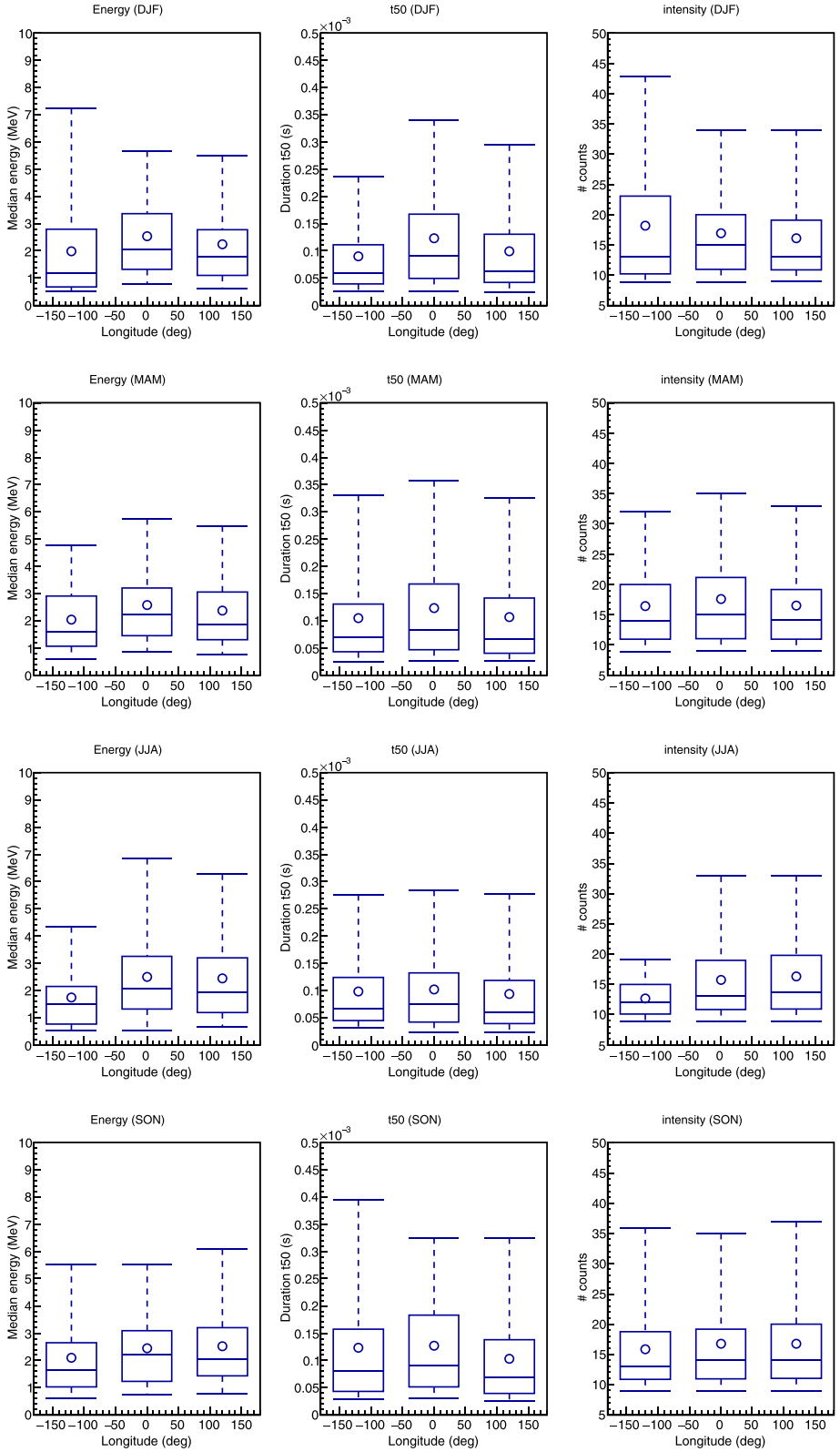

Figure 8. The trend of three characteristic parameters of TGFs: median energy (left panels), duration (center) and number of counts (right), for the three high-density regions and the four seasons. The top and bottom of the boxes represent the upper and lower quartiles of the distribution (75% and 25% of the data points). The end of the lower bar marks 5% of the data points and the end of the upper one marks 95%. The circle is the mean and the line in the box is the median of the distribution.

in the late afternoon compared to the other regions; this is consistent with the observed climatology of the area. Figure 7 presents an overview of all the events divided by the season in which they occur. As can be seen, a clear influence of seasons emerged with maximum at equinox and minimum in solstice. In terms of geographic distribution (panels on the left), we see that the peak over Africa is consistently the highest; this effect is explained by the equatorial orbit of AGILE (see also section 5.7), which covers the Congo basin, a very prolific area for thunderstorms. The number of events is particularly high in spring (March–May) and lowest in winter (December–February). However, during spring the Asian peak grows to almost the same level. The peak over Borneo is very visible in summer and fall (June-August and September-November), however, it is not a seasonal phenomenon: in the spring and fall months a small "bump" on the right of the Indonesian peak is visible. This bump has the same value as the Borneo peak in summer and winter, suggesting that the rate over Borneo is constant and is overpowered by the activity over Java and Sumatra in winter and spring. The fact that the local-time curve for Oceania has the same shape of the one for the other regions indicates that this peak over Borneo is not related to a specific kind of events. Another seasonal small peak is visible over the pacific in winter. This fourth lightning region was already reported in Fabró et al. (2015), but the scarcity of events in that region makes it difficult to draw any conclusions. Our findings are in accordance with the observations of the Optical Transient Detector, as reported in Christian et al. (2003) (see figure 6). The reported maximum of lightning activity in the period September–November over the Amazon basin is visible in our data also, even considering the low number of detected events. Christian et al. (2003) also report that the maximum of activity in Africa shifts from −20° latitude in December–February to +20° in June–August, following the Inter-Tropical Convergence Zone. However, such latitudes are outside the field of view of AGILE, and as a result we see our maximum of activity in March–May and September–November instead. Finally, in their figure 7, panel c, they also report a bimodal structure for the yearly activity rate, with maxima over April and October for the latitude band covered by AGILE; this is very well visible in Figure 4. The local time distributions (Figure 7, panels on the right) also show variations according to the time of the year. In particular, the imbalance between the rate in mornings and in evenings over Africa occurs in spring and fall, and a similar behavior is observed over Central America during fall; this trend seems to be reversed in summer over America. On the other hand, the detection rate in the mornings as opposed to the evenings seems to be comparable all year round in Oceania. Figure 8 shows a set of summary box plots for median energy (left), duration (center) and number of counts (right), divided for the four seasons and for the three lightning chimneys. There is no trend of such parameters with longitude or season; the small differences for the American peak are most likely due to the small number of events recorded there. Therefore, from this analysis, we conclude that there is no statistical evidence for variability of TGF properties such as median energy, duration and intensity with season and longitude, at least in the equatorial band. Therefore, we consider unlikely that our WI events, selected over spring and summer, are introducing a bias related to season in our sample.

5.7. Comparison With the Fermi Catalog

One of the distinct features of the AGILE sample is the dominance of the African peak, which is not observed by other missions; however, we interpret this feature as a product of the very narrow inclination of AGILE (2.5°). As a result, AGILE covers all the equatorial regions, particularly the Congo basin, while at the same time misses out other active regions, such as the Caribbean sea.

To show this, we plot the events from the Fermi catalog (Roberts et al., 2018) which occurred within ±2.5° of latitude and we see that their geographic and local time distributions are compatible with the ones obtained for the AGILE data set (Figure 9). Fermi data are available at https://fermi.gsfc.nasa.gov/ssc/data/access/gbm/tgf/; we used the Offline Search Table for this comparison. The latitude-based selection includes 454 out of 4,135 events detected within the period July 2008 to July 2016. There is thus only partial time overlap between AGILE and Fermi data sets. The African and Asian peaks are comparable between the two sets; so is the American one, but the data from AGILE show a little peak over the Pacific that is not present in the sample from Fermi, possibly due to the lower number of events in the sample. The differences in the local-time distributions are not significant.

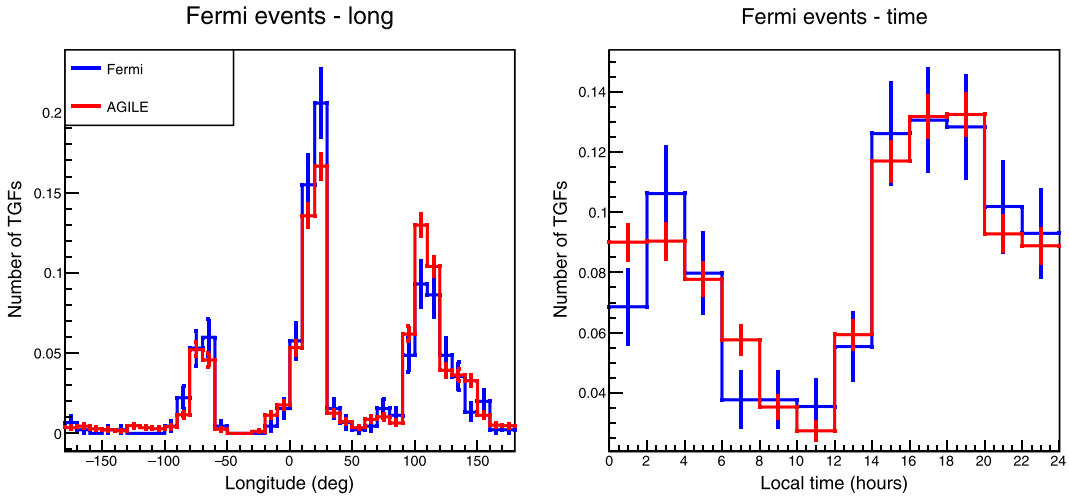

Figure 9. The geographic and local time distributions of AGILE ad Fermi data sets, superimposed and normalized for the total number of events.

6. Conclusions

The new catalog presented here contains 2,780 TGFs detected by AGILE over a 3-years span, and represents the largest data set of TGFs detected over the equatorial region (±2.5° of latitude) so far. The association with WWLLN showed that the selection criteria used for the previous catalogs were inadequate and the characteristics of WI TGFs were the base for the design of new criteria. After testing several sets of new criteria we selected the one that included the highest number of WI TGFs while at the same time maintaining the sample as clean as possible of false events. The reliability of the new sample was tested with the geographic and local-time distributions of the events and with the ratio between events occurring in stormy regions and events occurring in a selected control region. The characteristics of the new sample are consistent with previous observations, namely the Fermi catalog. The seasonal behavior for the various regions is consistent with the global annual lightning activity, reported by Christian et al. (2003); the TGF rate peaks at different times of the year in the different regions, according to local climate. Local weather patterns also influence the shape of the longitude distribution; in particular, the peak over Borneo was not visible in the previous catalogs, and it thus represents an additional improvement. Another active region that was previously undetected is the Pacific chimney. However, no trend related to location or season was found in energy, intensity or duration of the TGFs.

This catalog is openly accessible at this link: https://www.ssdc.asi.it/mcal3tgfcat, and it includes also the lightcurves of all events. The association of TGFs to lightning sferics detected by WWLLN is addressed in L20.

Acknowledgments
AGILE is a mission of the Italian Space Agency (ASI), with co-participation of INAF (Istituto Nazionale di Astrofisica) and INFN (Istituto Nazionale di Fisica Nucleare). This study was supported by the Research Council of Norway under contracts 208028/F50 and 223252/F50 (CoE). This project has received funding from the European Unions Horizon 2020 research and innovation program under the Marie Sklodowska-Curie grant agreement 722337. Some part of the simulations were performed on resources provided by UNINETT Sigma2 - the National Infrastructure for High Performance Computing and Data Storage in Norway, under project no. NN9526K. The authors wish to thank the World Wide Lightning Location Network (http://wwlln.net), a collaboration among over 50 universities and institutions, for providing the lightning location data used in this paper. The authors thank the International Space Science Institute, Bern, Switzerland, for providing financial support and meeting facilities in the frame of the International Team n. 471: *Understanding The Properties Of The Terrestrial Gamma-Ray Flash Population*. The data for the TGF sample presented in this work are publicly available at the ASI Space Science Data Center (SSDC) website (https://www.ssdc.asi.it/mcal3tgfcat).

References

Agostinelli, S. (2003). Geant4—A simulation toolkit. *Nuclear Instruments and Methods A*, *506*(3), 250–303.

Albrecht, R., Goodman, S., Buechler, D., Blakeslee, R., & Christian, H. (2016). LIS 0.1 Degree Very High Resolution Gridded Lightning Climatology Data Collection.

Briggs, M. S., Xiong, S., Connaughton, V., Tierney, D., Fitzpatrick, G., Foley, S., & Hutchins, M. L. (2013). Terrestrial gamma-ray flashes in the Fermi era: Improved observations and analysis methods. *Journal of Geophysical Research: Space Physics*, *118*, 3805–3830. https://doi.org/10.1002/jgra.50205

Carlson, B. E., Lehtinen, N. G., & Inan, U. S. (2007). Constraints on terrestrial gamma ray flash production from satellite observation. *Geophysical Research Letters*, *34*, 8. https://doi.org/10.1029/2006GL029229

Christian, H. J., Blakeslee, R. J., Boccippio, D. J., Boeck, W. L., Buechler, D. E., Driscoll, K. T., & Stewart, M. F. (2003). Global frequency and distribution of lightning as observed from space by the Optical Transient Detector. *Journal of Geophysical Research*, *108*(D1), 4005. https://doi.org/10.1029/2002JD002347

Chronis, T., Briggs, M. S., Priftis, G., Connaughton, V., Brundell, J., Holzworth, R., & Stanbro, M. (2016). Characteristics of thunderstorms that produce terrestrial gamma ray flashes. *Bulletin of the American Meteorological Society*, *97*(4), 639–653. https://doi.org/10.1175/BAMS-D-14-00239.1

Connaughton, V., Briggs, M. S., Xiong, S., Dwyer, J. R., Hutchins, M. L., Grove, J. E., & Wilson-Hodge, C. (2013). Radio signals from electron beams in terrestrial gamma ray flashes. *Journal of Geophysical Research: Space Physics*, *118*, 2313–2320. https://doi.org/10.1029/2012JA018288

Cummer, S. A., Lyu, F., Briggs, M. S., Fitzpatrick, G., Roberts, O. J., & Dwyer, J. R. (2015). Lightning leader altitude progression in terrestrial gamma-ray flashes. *Geophysical Research Letters*, *42*, 7792–7798. https://doi.org/10.1002/2015GL065228

Dwyer, J. R., & Cummer, S. A. (2013). Radio emissions from terrestrial gamma-ray flashes. *Journal of Geophysical Research: Space Physics*, *118*, 3769–3790. https://doi.org/10.1002/jgra.50188

Dwyer, J. R., & Smith, D. M. (2005). A comparison between Monte Carlo simulations of runaway breakdown and terrestrial gamma-ray flash observations. *Geophysical Research Letters*, *32*, L22804. https://doi.org/10.1029/2005GL023848

Fabró, F., Marisaldi, M., van der Velde, O. A., & Fuschino, F. (2015). Analysis of global terrestrial gamma ray flashes distribution and special focus on AGILE detections over South America. *Journal of Atmospheric and Solar-Terrestrial Physics*, *124*, 10–20. https://doi.org/10.1016/j.jastp.2015.01.009

Fishman, G. J., Bhat, P. N., Mallozzi, R., Horack, J. M., Koshut, T., Kouveliotou, C., & Christian, H. J. (1994). Discovery of intense gamma-ray flashes of atmospheric origin. *Science*, *264*(5163), 1313–1316.

Foley, S., Fitzpatrick, G., Briggs, M. S., Connaughton, V., Tierney, D., McBreen, S., & Wilson-Hodge, C. (2014). Pulse properties of terrestrial gamma-ray flashes detected by the Fermi Gamma-Ray Burst Monitor. *Journal of Geophysical Research: Space Physics*, *119*, 5931–5942. https://doi.org/10.1002/2014JA019805

Gjesteland, T., Østgaard, N., Collier, A. B., Carlson, B. E., Eyles, C., & Smith, D. M. (2012). A new method reveals more TGFs in the RHESSI data. *Geophysical Research Letters*, *39*, L05102. https://doi.org/10.1029/2012GL050899

Grefenstette, B. W., Smith, D. M., Hazelton, B. J., & Lopez, L. I. (2009). First RHESSI terrestrial gamma ray flash catalog. *Journal of Geophysical Research*, *114*, A02314. https://doi.org/10.1029/2008JA013721

Hazelton, B. J., Grefenstette, B. W., Smith, D. M., Dwyer, J. R., Shao, X. M., Cummer, S. A., & Holzworth, R. H. (2009). Spectral dependence of terrestrial gamma-ray flashes on source distance. *Geophysical Research Letters*, *36*, L01108. https://doi.org/10.1029/2008GL035906

Labanti, C., Marisaldi, M., Fuschino, F., Galli, M., Argan, A., Bulgarelli, A., & Trifoglio, M. (2009). Design and construction of the mini-calorimeter of the AGILE satellite. *Nuclear Instruments and Methods in Physics Research A*, *598*, 470–479. https://doi.org/10.1016/j.nima.2008.09.021

Lindanger, A., Marisaldi, M., Maiorana, C., Sarria, D., Albrechtsen, K., stgaard, N., Galli, M., Ursi, A., Labanti, C., Tavani, M., Pittori, C., & Verrecchia, F. (2020). The 3rd AGILE Terrestrial Gamma Ray Flash catalog. Part I: Association to lightning sferics. *Journal of Geophysical Research: Atmospheres*, *125*, e2019JD031985. https://doi.org/10.1029/2019JD031985

Mailyan, B. G., Briggs, M. S., Cramer, E. S., Fitzpatrick, G., Roberts, O. J., Stanbro, M., & Dwyer, J. R. (2016). The spectroscopy of individual terrestrial gamma-ray flashes: Constraining the source properties. *Journal of Geophysical Research: Space Physics*, *121*, 11,346–11,363. https://doi.org/10.1002/2016JA022702

Marisaldi, M., Argan, A., Ursi, A., Gjesteland, T., Fuschino, F., Labanti, C., & Gianotti, F. (2015). Enhanced detection of terrestrial gamma-ray flashes by AGILE. *Geophysical research letters*, *42*, 9481–9487. https://doi.org/10.1002/2015GL066100

Marisaldi, M., Fuschino, F., Labanti, C., Galli, M., Longo, F., Del Monte, E., et al. (2010). Detection of terrestrial gamma ray flashes up to 40 MeV by the AGILE satellite. *Journal of Geophysical Research*, *115*, A00E13. https://doi.org/10.1029/2009JA014502

Marisaldi, M., Fuschino, F., Tavani, M., Dietrich, S., Price, C., Galli, M., & Chen, A. (2014). Properties of terrestrial gamma ray flashes detected by AGILE MCAL below 30 MeV. *Journal of Geophysical Research: Space Physics*, *119*, 1337–1355. https://doi.org/10.1002/2013JA019301

Marisaldi, M., Galli, M., Labanti, C., Østgaard, N., Sarria, D., Cummer, S. A., & Verrecchia, F. (2019). On the high-energy spectral component and fine time structure of terrestrial gamma-ray flashes. *Journal of Geophysical Research: Atmospheres*, *124*, 7484–7497. https://doi.org/10.1029/2019JD030554

Mezentsev, A., Østgaard, N., Gjesteland, T., Albrechtsen, K., Lehtinen, N., Marisaldi, M., & Cummer, S. (2016). Radio emissions from double RHESSI TGFs. *Journal of Geophysical Research: Atmospheres*, *121*, 8006–8022. https://doi.org/10.1002/2016JD025111

Neubert, T., Østgaard, N., Reglero, V., Blanc, E., Chanrion, O., Oxborrow, C. A., & Bhanderi, D. D. V. (2019). The ASIM mission on the International Space Station. *Space Science Reviews*, *215*(2), 26. https://doi.org/10.1007/s11214-019-0592-z

Picone, J. M., Hedin, A. E., Drob, D. P., & Aikin, A. C. (2002). NRLMSISE-00 empirical model of the atmosphere: Statistical comparisons and scientific issues. *Journal of Geophysical Research*, *107*, 1468. https://doi.org/10.1029/2002JA009430

Roberts, O. J., Fitzpatrick, G., Stanbro, M., McBreen, S., Briggs, M. S., Holzworth, R. H., & Mailyan, B. G. (2018). The First Fermi-GBM Terrestrial Gamma Ray Flash Catalog. *Journal of Geophysical Research: Space Physics*, *123*, 4381–4401. https://doi.org/10.1029/2017JA024837

Smith, D. M., Lopez, L. I., Lin, R. P., & Barrington-Leigh, C. (2005). Terrestrial gamma-ray flashes observed up to 20 MeV. *Science (New York, N.Y.)*, *307*, 1085–1088. https://doi.org/10.1126/science.1107466

Tavani, M., Barbiellini, G., Argan, A., Boffelli, F., Bulgarelli, A., Caraveo, P., & Giacomazzo, M. (2009). The AGILE mission. *Astronomy and Astrophysics*, *502*(3), 995–1013. https://doi.org/10.1051/0004-6361/200810527

Ursi, A., Tavani, M., Verrecchia, F., Marisaldi, M., Argan, A., Trois, A., & Tempesta, P. (2019). A new AGILE MCAL configuration to detect gamma-ray bursts and sub-threshold events in the multimessenger era. *The Astrophysical Journal*, *871*(1), 27. https://doi.org/10.3847/1538-4357/aaf28f